Retinal lipid and glucose metabolism dictates angiogenesis through the lipid sensor Ffar1

The Harvard community has made this article openly available. Please share how this access benefits you. Your story matters

Citation	Jean-Sébastien Joyal, Ye Sun, Marin L Gantner, Zhuo Shao, Lucy P Evans, Nicholas Saba, Thomas Fredrick, Samuel Burnim, Jin Sung Kim, Gauri Patel, Aimee M Juan, Christian G Hurst, Colman J Hatton, Zhenghao Cui, Kerry A Pierce, Patrick Bherer, Edith Aguilar, Michael B Powner, Kristis Vevis, Michel Boisvert, Zhongjie Fu, Emile Levy, Marcus Fruttiger, Alan Packard, Flavio A Rezende, Bruno Maranda, Przemyslaw Sapieha, Jing Chen, Martin Friedlander, Clary B Clish, & Lois E H Smith. 2016. Retinal lipid and glucose metabolism dictates angiogenesis through the lipid sensor Ffar1. Nature Medicine 22: 439–445. doi: 10.1038/nm.4059
Published Version	10.1038/nm.4059
Citable link	http://nrs.harvard.edu/urn-3:HUL.InstRepos:33766542
Terms of Use	This article was downloaded from Harvard University's DASH repository, and is made available under the terms and conditions applicable to Open Access Policy Articles, as set forth at http://nrs.harvard.edu/urn-3:HUL.InstRepos:dash.current.terms-of-use#OAP

Retinal lipid and glucose metabolism dictates angiogenesis through lipid sensor Ffar1

Jean-Sébastien Joyal[1,2,3,†], **Ye Sun**[3], **Marin L. Gantner**[5], **Zhuo Shao**[4], **Lucy P. Evans**[4], **Nicholas Saba**[4], **Thomas Fredrick**[4], **Samuel Burnim**[4], **Jin Sung Kim**[3], **Gauri Patel**[2], **Aimee M. Juan**[3], **Christian G. Hurst**[4], **Colman J. Hatton**[4], **Zhenghao Cui**[4], **Kerry A. Pierce**[6], **Patrick Bherer**[7], **Edith Aguilar**[8], **Michael B. Powner**[9], **Kristis Vevis**[9], **Michel Boisvert**[10], **Zhongjie Fu**[4], **Emile Levy**[10], **Marcus Fruttiger**[9], **Alan Packard**[11], **Flavio A. Rezende**[12], **Bruno Maranda**[7], **Przemyslaw Sapieha**[12], **Jing Chen**[4], **Martin Friedlander**[8], **Clary B. Clish**[6], and **Lois E.H. Smith**[4,†]

[1]Department of Pediatrics, CHU Sainte-Justine Research Center, Université de Montréal, Montreal, Qc, Ca

[2]Department of Pharmacology, CHU Sainte-Justine Research Center, Université de Montréal, Montreal, Qc, Ca

[3]Department of Pharmacology and Therapeutics, McGill University, Montreal, Qc, Ca

[4]Department of Ophthalmology, Harvard Medical School, Boston Children's Hospital, MA, USA

[5]The Lowy Medical Research Institute, La Jolla, CA, USA

[6]Metabolite Profiling Platform, The Broad Institute of MIT and Harvard University, Cambridge, MA, USA

[7]Department of Genetics, Université de Sherbrooke, Sherbrooke, Qc, Ca

[8]Department of Cell and Molecular Biology, The Scripps Research Institute, La Jolla, CA, USA

[9]Institute of Ophthalmology, University College London, London, UK

[10]Department of Nutrition, CHU Sainte-Justine Research Center, Université de Montreal, Montreal, Qc, Ca

[11]Radiology, Harvard Medical School, Boston Children's Hospital, MA. USA

†Correspondence should be addressed to: Lois E. H. Smith, M.D., Ph.D., Harvard Medical School, Children's Hospital Boston, Tel: 617-355-8531 ; Email: lois.smith@childrens.harvard.edu, Otherwise to: Jean-Sébastien Joyal, M.D., Ph.D., CHU Sainte-Justine Research Center, Université de Montreal, Tel: 514-345-3317 ; Email: js.joyal@umontreal.ca

COMPETING FINANCIAL INTERESTS

The authors declare no competing financial interests.

[12]Department of Ophthalmology, Maisonneuve-Rosemont Hospital Research Centre, Université de Montréal, Montreal, Qc, Ca

Abstract

Tissues with high metabolic rates often use lipid as well as glucose for energy, conferring a survival advantage during feast and famine.[1] Current dogma suggests that high-energy consuming photoreceptors depend on glucose.[2,3] Here we show that retina also uses fatty acids (FA) β-oxidation for energy. Moreover, we identify a lipid sensor Ffar1 that curbs glucose uptake when FA are available. Very low-density lipoprotein receptor (VLDLR), expressed in tissues with a high metabolic rate, facilitates the uptake of triglyceride-derived FA.[4,5] Vldlr is present in photoreceptors.[6] In $Vldlr^{-/-}$ retinas, Ffar1, sensing high circulating lipid levels despite decreased FA uptake[5], suppresses glucose transporter Glut1. This impaired glucose entry into photoreceptors results in a dual lipid/glucose fuel shortage and reduction in the Krebs cycle intermediate α-ketoglutarate (KG). Low α-KG levels promote hypoxia-induced factor-1α (Hif1a) stabilization and vascular endothelial growth factor (Vegfa) secretion by starved $Vldlr^{-/-}$ photoreceptors, attracting neovessels to supply fuel. These aberrant vessels invading normally avascular photoreceptors in $Vldlr^{-/-}$ retinas are reminiscent of retinal angiomatous proliferation (RAP), a subset of neovascular age-related macular degeneration (AMD)[7], associated with high vitreous VEGF levels in humans. Dysregulated lipid and glucose photoreceptor energy metabolism may therefore be a driving force in neovascular AMD and other retinal diseases.

Retinal neovascularization (RAP) is seen in macular telangiectasia (MacTel)[8] as well as in 15–20% of macular neovascular age-related macular degeneration (AMD)[7], the leading cause of blindness in older adults.[9] Photoreceptors, densest in the macula, are amongst the highest energy consuming and mitochondria-rich cells[2,10] consistent with high-energy demands causing macular neovascularization. VEGF contributes to retinal neovascularization, but factors that initiate VEGF secretion in macular disease remain largely unknown. We hypothesized that disordered photoreceptor mitochondrial energy metabolism might drive aberrant angiogenesis in the normally avascular photoreceptors in an attempt to increase fuel supply, consistent with dyslipidemia and mitochondrial dysfunction (associated with aging) being important risk factors of neovascular AMD.[9]

Retinal neurons are thought to rely on glucose for fuel.[2,3] Glucose is metabolized to pyruvate (by glycolysis) and either converted to lactate in cytosol, or oxidized into acetyl-CoA in mitochondria before entering the Krebs cycle to produce ATP. In photoreceptors, the major glucose transporter is GLUT1.[11,12] Clinically, $GLUT1$ deficiency causes infantile seizures and developmental delay[13], highlighting the importance of glucose metabolism in brain. However, $GLUT1$ deficient individuals have normal vision suggesting alternative retinal energy substrates, perhaps through lipid β-oxidation.

Lipid β-oxidation is common in heart and skeletal muscle with high metabolic rates, where abundant VLDLR facilitates fatty acid (FA) uptake.[14] VLDLR binds chylomicrons and enables cleavage of long-chain FA from triglycerides (TG) by lipoprotein lipase.[5] VLDLR fosters transcytosis of active lipoprotein lipase across endothelial cells[15], to deliver free FA to tissue. $Vldlr$ deletion suppresses lipid uptake and FA β-oxidation in the heart.[4] We

hypothesized a similar mechanism in Vldlr-rich, and lipid-rich photoreceptors. Lipid β-oxidation enzymes are expressed in the eye.[16] Clinically, *VLDLR* deletion causes maculopathy[17] and *Vldlr*^{−/−} mice develop RAP-like retinal vascular lesions (Fig. 1a).[6] *Vldlr*^{−/−} mice allow exploration of the hypotheses that lipids fuel photoreceptors and fuel deficiency promotes neovessels.

We first linked the number of RAP-like lesions to photoreceptor energy demand. Rod photoreceptors consume 3–4 times more energy in darkness than in light to maintain the 'dark current', an electrochemical gradient required for photon-induced depolarization.[10] Conversely, membrane turnover and visual cycle activity are decreased in darkness.[10] Dark-raised *Vldlr*^{−/−} mice developed 1.5 fold more RAP-like vascular lesions than light/dark cycle-raised mice (Fig. 1b), suggesting that energy metabolism influences neovascular disease. Photoreceptors mature from the optic nerve outward towards the periphery. Energy consumption increases as photoreceptors mature and at P16 the more mature central retina had more RAP-like lesions.[2,18]

To determine if Vldlr loss specifically in photoreceptors was sufficient to drive pathological vessels, we selectively knocked down remaining *Vldlr* in photoreceptors (using AAV2-hRK) in *Vldlr*^{+/−} mice with normal circulating fatty acid levels.[19] RAP-like lesions developed with *Vldlr* loss in photoreceptors alone (Supplementary Fig. 1). Consistent with energy deficiency, *Vldlr*^{−/−} photoreceptors had swollen mitochondria (3D scanning electron microscopy, Fig. 1c, Supplementary Videos 1,2). Moreover, *Vldlr*^{−/−} retinas had lower ATP stores (Fig. 1d), confirming an energy deficit.

To explore the etiology of energy deficit fostering neovascularization, we examined the contribution of FA and glucose to WT retinal energy production (Supplementary Fig. 2a). The long-chain FA palmitate fueled mitochondrial β-oxidation in retinal explants, doubling oxygen consumption rates (OCR). Etomoxir-induced inhibition of FA transport into mitochondria abrogated mitochondrial respiration, confirming that FA β-oxidation contributes to retinal energy metabolism (Fig. 2a,b, Supplementary Fig. 2a–c). We also examined the contribution of glucose oxidation and found that retinal glucose could be oxidized by mitochondria as efficiently as FA (Supplementary Fig. 2d–f). However, as reported by Warburg, Cohen and Winkler[3,20], the vast majority of glucose (87%) was converted to lactate by glycolysis rather than oxidative phosphorylation (Supplementary Fig. 2g). Unlike WT, *Vldlr*^{−/−} retinas (with limited FA uptake) did not increase mitochondrial respiration when exposed to palmitate (Supplementary Fig. 2h). FA therefore contributes to retinal energy production in addition to glucose and may be deficient in *Vldlr*^{−/−} retinas.

In view of the possible role of Vldlr in retinal lipid energy metabolism, we quantified retinal FA uptake. *Vldlr* as reported was highly expressed in retinal photoreceptors (Supplementary Fig. 3a).[21] Retinal mid/long-chain FA uptake was reduced in *Vldlr*^{−/−} retinas. Serum turbidity reflected higher circulating lipid levels (Supplementary Fig. 3b,c). Triglycerides and mid/long-chain FA plasma levels (particularly palmitate) were elevated in *Vldlr*^{−/−} mice (Fig. 2c, Supplementary Fig. 3d,e). Importantly, FA β-oxidation of lipids in mitochondria to produce acetyl-CoA was suppressed (Fig. 2d). In *Vldlr*^{−/−} retinas, total acylcarnitine and free carnitine levels were reduced (Fig. 2e). Low cytosolic FA levels were associated with

decreased peroxisome proliferative activated receptor alpha (*Ppara*) expression[22], mainly in *Vldlr*^{−/−} photoreceptors (Supplementary Fig. 4a,b). Ppara is a key regulator of several steps of FA β-oxidation[22], including Cpt1a that mediates internalization of FA into mitochondria (Supplementary Fig. 2a). *Cpt1a* was enriched in WT but suppressed in *Vldlr*^{−/−} photoreceptors (Fig. 2f). A selective Ppara agonist (WY16463) used to enhance FA β-oxidation[23], reduced RAP-like lesions in *Vldlr*^{−/−} retina (Supplementary Fig. 4c). Providing photoreceptor (661W) cells with palmitate alone or with Ppara agonist (GW9578) further increased mitochondrial respiration by FA β-oxidation and not via uncoupling, since etomoxir abrogated the increase in respiration (Supplementary Fig. 5a–d). Extracellular acidification rates, reflecting lactate production from glycolysis, were not affected by a Ppara agonist (Supplementary Fig. 5e,f). Further exploration of the role of Ppara in metabolic signaling in neovascular eye disease is warranted. Collectively, our findings suggest that lipids are an energy substrate in retina, challenging the current dogma that glucose is the only fuel of photoreceptors.

We initially anticipated a compensatory upsurge in glucose uptake to mitigate FA deficiency in *Vldlr*^{−/−} retinas. Surprisingly, retinal glucose uptake (^{18}F-FDG) assessed by positron emitting tomography (PET) and retinal ^{18}F-FDG counts was reduced compared to WT (Fig. 2g, Supplementary Video 3), as was Glut1 expression (Fig. 2h,i), particularly in *Vldlr*^{−/−} photoreceptors (Fig. 2h). In accord, carbohydrate metabolism was the most significantly regulated pathway on a gene microarray comparing *Vldlr*^{−/−} to WT retinas (Supplementary Fig. 6a). The suppression of pyruvate kinase (*Pkm2*), a critical enzyme of glycolysis was identified by the array and confirmed by qRT-PCR (Supplementary Fig. 6b). Glut3 and 4 were not regulated (Supplementary Fig. 6c). Hence, *Vldlr*^{−/−} retinas have both lipid and glucose uptake deficiencies (Fig. 2) consistent with a generalized energy shortage (Fig. 1).

We posited that an abundance of lipids in *Vldlr*^{−/−} serum might signal through lipid sensors to reduce glucose uptake and help control fuel supply to the retina (Fig. 3a). We screened for known FA-sensing G-protein coupled membrane receptors (GPCR) in retina. *Ffar1* was the most abundantly expressed FA receptor in WT and increased further in *Vldlr*^{−/−} retinas, particularly in photoreceptors (Fig. 3b,c). Ffar1, first discovered in pancreas[24], governs glucose transport and insulin secretion in β-islet cells.[25,26] High pancreatic Ffar1 expression suppresses expression of the main endocrine pancreas glucose transporter, Glut2.[27] Ffar1 has also been localized in brain, where its function is ill defined.[28,29] In WT and *Vldlr*^{−/−} retinas, we found that a Ffar1 agonist (GW9508) suppressed the expression of Glut1[12] and retinal glucose uptake (Fig. 3d,e, Supplementary Fig. 7a). Importantly, treatment with Ffar1 agonist (GW9508) more than doubled the number of RAP-like lesions in *Vldlr*^{−/−} retinas compared to controls (Fig. 3f). Ffar1 binds lipids comprising more than 6 carbons.[29] *Vldlr*^{−/−} mice treated with Ffar1 lipid agonists medium chain triglycerides (MCT; 8–10 carbons)[29] or a second Ffar1 selective agonist TAK-875[30] had increased *Glut1* suppression and more RAP-like lesions versus controls (Supplementary Fig. 8). Deletion of *Ffar1* in *Vldlr*^{−/−} mice raised retinal glucose uptake (Fig. 3g, Supplementary Video 3) and Glut1 expression towards WT and *Ffar1*^{−/−} levels (Fig. 3h; Supplementary Fig. 7b,c), with fewer RAP-like lesions in *Vldlr*^{−/−}/*Ffar1*^{−/−} mice (Fig. 3i). *In vitro*, knocking down *Ffar1* or treating cells with MEK/ERK inhibitor (PD98059) prevented *Glut1* suppression by GW9508 in photoreceptors

(661W; Supplementary Fig. 7d–f). Therefore, Ffar1 may act as nutrient sensor, coupling mitochondrial metabolism with circulating substrate availability.

We hypothesized that photoreceptors challenged by a dual glucose and lipid fuel substrate deficiency would signal to increase vascular supply, in an attempt to restore energy homeostasis (Fig. 4a). Hypoxia has been assumed to be the main driver of angiogenesis, but inadequate nutrient availability to tissue might also control blood vessel growth. We found a reduction in pyruvate level, a metabolic intermediate feeding into the Krebs cycle from decreased glucose uptake and glycolysis (Fig. 4b) and also less acetylcarnitine from decreased FA uptake and β-oxidation (Fig. 4c) associated with less α-ketoglutarate (α-KG), an essential intermediate (Fig. 4d). Together with oxygen, α-KG is a necessary co-activator of propyl-hydroxylase dehydrogenase (PHD) that tags Hif1a for degradation by proline hydroxylation.[31] Less hydroxyproline was detected in *Vldlr*^{−/−} retinas, consistent with reduced PHD activity (Fig. 4e). Indeed, reduction in retinal glucose uptake by Ffar1 agonist GW9508 and glucose starvation in photoreceptors (661W) was associated with Hif1a stabilization (Supplementary Fig. 9a–c) and Vegfa secretion (Supplementary Fig. 9d,e). *In vivo*, Hif1a stabilization (Fig. 4f) in *Vldlr*^{−/−} photoreceptors (Fig. 4g) was associated with Vegfa production (Fig. 4h,i). Deletion of *Ffar1* in *Vldlr*^{−/−} retinas suppressed Hif1a stabilization and *Vegfa* secretion (Fig. 4f,h), leading to fewer vascular lesions (Fig. 3i). Consistent with our results[32], mice engineered to secrete Vegfa in photoreceptors develop retinal angiomatous proliferation comparable to *Vldlr*^{−/−} mice[33]; Vegfa from photoreceptors is therefore sufficient to promote RAP-like lesions. Importantly, oxidative stress associated with an energy crisis may also directly stabilize Hif1a and promote Vegfa secretion in *Vldlr*^{−/−} photoreceptors[6,34,35], potentially contributing to vascular lesions. However, macrophages, often implicated in the etiology of AMD, were not associated with the onset of development of nascent RAP-like lesions, surrounding only mature vascular lesions (Supplementary Fig. 10). Translating these findings to human disease, higher vitreous VEGF levels were detected in AMD/RAP human subjects compared to controls (macular hole; Fig. 4j). These findings imply that lipid/glucose fuel insufficiency in retina, in part through reduction of Krebs cycle metabolite α-KG, can drive aberrant angiogenesis in the normally avascular photoreceptor layer.

In the retina, the ability to use both lipids and glucose as fuel, might be beneficial in periods of high fuel need or fuel deprivation. Fasting liberates FA from adipose tissue that is used by high-energy consuming organs capable of FA β-oxidation such as heart, and perhaps retina (Fig. 2a–f, Supplementary Fig. 2a–c, Supplementary Fig. 5a–d). Indeed, FA β-oxidation disorders are associated with retinopathy.[36] Tissues that use lipid as fuel curb glucose uptake during starvation.[1,37] The capacity to sense nutrient availability and adapt fuel uptake might improve metabolic efficiency. G-protein coupled receptors (GPCR) are known membrane sensors of amino acids, glucose and lipids.[38] Here we show that Ffar1 is a metabolic sensor of FA availability, which controls glucose entry into the retina (Fig. 3). We speculate that long-term suppression of glucose entry by Ffar1 in photoreceptors (perhaps secondary to circulating lipids) might contribute to age-related mitochondrial dysfunction in AMD or MacTel. Retinal effects of Ffar1 agonists considered for the treatment of type II diabetes should be carefully monitored, particularly in older individuals at increased risk of AMD.

Mitochondrial metabolism may contribute to pathological angiogenesis in other diseases, such as cancer. To provide building blocks for proliferation, tumors promote angiogenesis at the cost of efficient ATP production by the *Warburg effect*.[39] In suppressing mitochondrial oxidative phosphorylation, tumor cells may generate less α-KG[31,40]. This inhibits prolyl-hydroxylase dehydrogenase (PHD) with ensuing HIF-1α stabilization, driving tumor angiogenesis required for growth. Our findings suggest the importance of mitochondrial fuel starvation as a driver of angiogenesis, matching energy demands with vascular supply. With a decline in mitochondrial function with age, this process may contribute to pathological angiogenesis in diseases of aging retina.

In summary, we show that lipid uptake and lipid β-oxidation are curtailed in *Vldlr*$^{-/-}$ retinas. Increased circulating FA can activate Ffar1, associated with decreased retinal glucose uptake and decreased Kreb cycle intermediate α-KG. Hif1a is stabilized and Vegfa secreted by *Vldlr*$^{-/-}$ photoreceptors, giving rise to pathologic RAP-like neovessels. This study uncovered three important novel mechanisms contributing to retinal physiology and neovascular AMD/RAP: (1) lipid β-oxidation is an energy source for the retina, (2) Ffar1 is an important nutrient sensor of circulating lipids that controls retinal glucose entry to match mitochondrial metabolism with available fuel substrates, and (3) nutrient scarcity is a driver of retinal pathological angiogenesis. These pathways may be important for discovery of new therapeutics.

ONLINE METHODS

Animals

All studies adhered to the NIH guide for the Care and Use of laboratory animals, the Association for Research in Vision and Ophthalmology (ARVO) Statement for the Use of Animals in Ophthalmic and Vision Research and were approved by the Institutional Animal Care and Use Committee at Boston Children's Hospital. *Vldlr* knockout mice (*Vldlr*$^{-/-}$; Jackson Lab Stock: 002529) were crossed with wild type C57Bl/6 mice to obtain heterozygous breeders for littermate controlled experiments. *Vldlr*$^{-/-}$ mice were also crossed with *Ffar1* knockout mice (*Ffar1*$^{-/-}$)[1] to ultimately obtain *Vldlr*$^{-/-}$/*Ffar1*$^{-/+}$ heterozygous breeders and double knockout mice (*Vldlr*$^{-/-}$/*Ffar1*$^{-/-}$). Pups weighing less than 5 grams or more than 7 grams at postnatal day (P)16 were excluded.[41] Littermate *Vldlr*$^{-/-}$ pups were treated from P8 to P15 with WY164363 (50mg/kg once daily, intraperitoneal; Sigma), GW9508 (14 μM, once daily intraperitoneal; Cayman), TAK–875 (15 mg/kg twice daily, gavage; Selleckchem), medium chain triglyceride oil (MCT, 20μL once daily gavage; Nestle) or corresponding vehicle and sacrificed at P16 to quantify retinal vascular lesions. Mice pups of both genders were used.

Quantification of vascular lesions

For quantification of outer retina vascular lesions, reminiscent of retinal angiomatous proliferation (RAP) or macular telangiectasia (MacTel), mice were euthanized with a mixture of xylazine and ketamine and eyes were enucleated and fixed in 4% paraformaldehyde for 1 h at room temperature. Retinas were dissected, carefully removing all hyaloid vessels, and stained overnight at room temperature with fluoresceinated Isolectin

B_4 (lectin) (Alexa Fluor 594 – I21413, Molecular Probes) in 1 mM $CaCl_2$ in PBS. Lectin-stained retinas were whole-mounted onto Superfrost/Plus microscope slides (Fisher Scientific) with the photoreceptor side up and embedded in SlowFade Antifade reagent (Invitrogen). For quantification of retinal lesions 20 images of each whole-mounted retina were obtained at 10× magnification on a Zeiss AxioObserver.Z1 microscope and merged to form one image using AxioVision 4.6.3.0 software. Vascular lesion counts were analyzed using the SWIFT_MACTEL method, an adaptation of the method used to measure neovascularization (SWIFT_NV)[42] in the oxygen induced retinopathy model.

SWIFT_MACTEL

We created a set of macros that was developed to run on ImageJ platform (National Institutes of Health, http://imagej.nih.gov/ij/). In brief, SWIFT_MACTEL isolates the red channel from a lectin-stained retinal whole mount, divides the image into four quadrants and removes background fluorescence to allow for the neovascularization (NV) structures to stand out clearly against the background fluorescence of normal vessels. Using a slide bar to either increase or decrease a particular quadrant's fluorescence threshold, the SWIFT_MACTEL user designates a threshold that marks NV structures but not normal vessels to each quadrant. After setting the appropriate threshold, artifacts like cellular debris or hyperfluorescent retinal edges can be manually removed and excluded from quantification. SWIFT_MACTEL then analyzes all pixels in the image that lie above the chosen intensity threshold and are part of an object that has a minimum size of 100 pixels. By setting this cut-off in object size, small artifacts like vessel branch points are automatically removed. After measuring all four quadrants, SWIFT_MACTEL creates a composite from all four NV quadrants and calculates the total NV pixel number. Results from the SWIFT_NV method have been found to correlate well with results from the established hand measurement protocols ($R^2 = 0.9372$) and show robust intra-individual ($R^2 = 0.9376$) and inter-individual ($R^2 = 0.9424$) reproducibility[42]. n is number of eyes quantified.

Scanning electron microscopy and 3D retinal reconstruction

Tissue was processed for serial block face scanning electron microscopy (SEM) using an adapted version of a protocol established by Deerinck et al 2010[5]. Whole eyes were isolated and fixed in Karnovsky's fixative. The cornea and lens were removed and the tissue further fixed in tannic acid overnight. Heavy metal infiltration was then undertaken; tissue was incubated in 1.5% potassium ferrocyanide, 0.5% osmium tetroxide in cacodylate buffer, followed by thiocarbohydrazide treatment and a second exposure to 1% osmium incubation. Walton's lead aspartate exposure was not carried out, so they were finished with 1% uranyl acetate incubation followed by dehydration to propylene oxide and embedded in Durcupan ACM resin. The tissue was serially sectioned and imaged using the Gatan 3VIEW serial block face imaging system (Gatan, Abingdon, UK) fitted to a Zeiss Sigma variable pressure field emission scanning electron microscope (Zeiss, Cambridge, UK). Data was collected and used in Amira Software (FEI, Oregon, USA) in order to reconstruct the 3D images. Using the same software, photoreceptor mitochondrial volume was estimated for WT mice, around the lesions in *Vldlr*^{−/−} mice, and away from the lesion in *Vldlr*^{−/−} mice.

ATP measurement

ATP was measured using a kit per instruction manual (Molecular Probes, A22066). Briefly, a standard reaction solution was made from the following components: dH_2O, 20× Reaction Buffer, DTT (0.1 M), D-luciferin (10 mM), firefly luciferase stock solution (5 mg/mL). Low-concentration ATP standard solutions were prepared by diluting ATP solution (5 mM) in dH_2O. A standard curve was generated by subtracting the background luminescence of the standard reaction solution from luminescence readings for a series of dilute ATP standard solutions. Luminescence measurements were taken for ATP-containing samples and the amount of ATP in experimental samples were calculated from the standard curve.

Oxygen consumption and extracellular acidification rates

All oxygen consumption rates were measured using a Seahorse XF^{e}96 Flux Analyzer®. Whole retinas were isolated and 1 mm punch biopsies were loaded into the 96 well plate. Retinal punches were incubated in assay media (DMEM 5030 media supplemented with 12 mM glucose, 10 mM HEPES and 26 mM $NaHCO_3$) to measure oxygen consumption rates (OCR) and extracellular acidification rates (ECAR). Photoreceptor (661W) cells, were incubated in their assay media (DMEM 5030, 12 mM glucose, 10 mM HEPES) one hour prior to measurements. Fatty acid oxidation rates were determined by treating tissues or cells with Etomoxir (40 μM; Sigma) 40 min prior to analysis and then providing BSA (control) or BSA/Palmitate conjugate (Seahorse). Glucose oxidation rates were measured after injection of 2-deoxyglucose (2-DG, 100 mM; Sigma) or media control during data acquisition. To determine the maximal fatty acid or glucose oxidative capacity, the non-mitochondrial respiration (rate after injection of 2 μM Rotenone and 2 μM Antimycin A) was subtracted from the oxygen consumption rate after injection of 0.5 μM carbonyl cyanide-*p*-trifluoromethoxyphenylhydrazone (FCCP).

Glucose and lactate measurements

Whole retinas and photoreceptors (661W) were incubated in assay media (DMEM 5030, 12 mM glucose, 10 mM HEPES) for 6 and 48 hours respectively. Media was collected, spun briefly (13 g) to remove cellular debris, and glucose and lactate levels measured using a Yellow Springs Instrument (YSI) 2950 were compared to control media that was not exposed to tissue or cells. To determine the conversion of glucose to lactate (the glycolytic rate), lactate production was divided by glucose uptake.

Retinal lipid uptake

We compared retinal long-chain fatty acid uptake of wild type and *Vldlr*$^{-/-}$ mice gavaged with 0.1 mg of 4,4-difluoro-5,7-dimethyl-4-bora-3a, 4a-diaza-s-indacene-3-hexadecanoic acid (BODIPY FL C16; Molecular Probes). Mice were euthanized 2 h later and the eyes were enucleated, embedded in OCT and cryo-sectioned (10 μm) for immediate imaging by fluorescence microscopy. Retinal FA uptake was quantitated using ^{14}C-labeled 2-bromopalmitate tracer injected twice daily (i.p.; 0.5 uCi per dose) from P9 to P12; total administered radioactivity was normalized for mouse body weight. Retinas were then dissected and homogenized in Ultima Gold liquid scintillation cocktail (PerkinElmer) and

beta-counted (^{14}C DPM) using Tri-Carb 2900TR instrument (PerkinElmer), correcting for background scintillation.

Plasma triglycerides (TG) and fatty acid (FA) analysis

Plasma was isolated from WT and $Vldlr^{-/-}$ mice by centrifugation (2000 g × 20 min; 4 °C) of whole blood in EDTA-coated tubes. TG were determined using the RANDOX TRIGS kit (TR210) per instruction manual. FAs in whole plasma were assayed as described previously.[43] Briefly, each sample was subjected to direct trans-esterification and then injected into a gas chromatograph using the Agilent GC AutoSampler system (7890A). FAs were identified by comparison with the expected retention times of known standards and then analyzed with OpenLAB Software Suite (Agilent).

β-Oxidation metabolite quantification

Acylcarnitine metabolites were extracted from WT and $Vldlr^{-/-}$ (P12) flash frozen retinas using ice-cold methanol. Samples were sonicated, centrifuged and the supernatant was transferred to a fresh tube for nitrogen evaporation. When dry, butanolysis was performed (butanol-HCl, 55°C for 20 min) prior to reconstitution in mobile phase (ACN:H_2O 80:20, formic acid 0.05%). Samples were analyzed by liquid chromatography followed by tandem mass spectrophotometry (LC/MS/MS, Alliance 2795 LC and Quattro micro, Waters Corp). Data were recorded in positive electrospray ionization and analyzed with Neolynx (Waters Corp).

Retinal glucose uptake

Positron emission tomography (PET) imaging studies were performed on WT, $Vldlr^{-/-}$, $Vldlr^{-/-}/Ffar1^{-/-}$ and $Ffar1^{-/-}$ mice (P16; Focus 120 high-resolution, Siemens), followed by micro CAT imaging (MicroCAT II scanner, Siemens). Fluorine-18 fluorodeoxyglucose (^{18}F-FDG) was administered by intraperitoneal injection (i.p.) to obtain non-toxic radioactivity levels (3.7 and 37 MBq; or 0.1 to 1.0 mCi). Actual administered activity was determined using a dose calibrator to measure activity in the syringe before and after the injection. Images were acquired 60 minutes after injection to ensure radiotracer uptake. Mice were fasted for 6 hours prior to imaging, kept in darkness and anesthetized by inhalation of isoflurane (2–4%) through a nose cone for the duration of the procedure. Animals were imaged in a head first, prone position, and placed on a heating pad to maintain appropriate body temperature. Upon completion of imaging, mice were euthanized and retinas were dissected for precise ^{18}F-FDG retinal activity, quantification by gamma counter, and corrected for decay. WT and $Vldlr^{-/-}$ mice pups were also injected with trace amounts of ^{3}H-2-deoxyglucose (0.5 μCi daily, i.p.) and treated with GW9508 or vehicle (14 μM daily, i.p.) for 5 days (P7–P12). Retinas were collected and homogenized in a scintillation cocktail (Ecolite +, MP biomedicals) and beta-counts measured using the LS6500 Multipurpose Scintillation Counter (Beckman).

Laser-capture microdissection

Eyes were embedded in OCT and flash frozen immediately following enucleation. Eyes were cryosectioned under RNase free conditions into 10 μm sections, and collected on

RNase-free polyethylene naphthalate glass slides (11505189, Leica). Sections were stained for lectin (1:50 in 1 mM $CaCl_2$) and dehydrated with 70%, 90% and 100% ethanol washes. Retinal vessels and layers were microdissected with a Leica LMD 6000 system (Leica Microsystems) and collected directly into RNA stabilizing buffer from the RNeasy Micro kit (Qiagen, Chatsworth, CA). RNA was extracted from microdissected tissues using the RNeasy Kit as described above (Qiagen), and real-time PCR was performed with the generated cDNA.

Reverse transcription and quantitative real-time PCR analysis

RNA samples from cell culture, whole retina or laser-captured neovessels and layers were treated with DNase I (Qiagen, Chatsworth, CA) to remove any contaminating genomic DNA. The DNase-treated RNA was then converted into cDNA using reverse transcriptase (Invitrogen). PCR primers for target genes and the control gene, *cyclophilin A*, were designed using Primer Bank and NCBI Primer Blast software. Quantitative analysis of gene expression was generated using an ABI Prism 7700 Sequence Detection System with the SYBR Green Master mix kit and gene expression was calculated relative to *cyclophilin A* using the cT method.

Expression Array

Illumina mouse gene microarray analysis of WT and *Vldlr*^{−/−} retinas was performed in biological triplicate (Mouse-WG6 expression BeadChip, Illumina). The chip contains 45,000 probe sets representing 34,000 genes. Microarray studies, from cDNA synthesis to raw data normalization were performed by the Molecular Genetics Core Facility at Boston Children's Hospital. Briefly, total RNA (1 μg each) was reverse transcribed, followed by a single in vitro transcription amplification to incorporate biotin-labeled nucleotide, and subsequent hybridization and staining with strepatavidin-Cy3 according to the manufacturer's instructions. The chip was scanned with Illumina BeadArray Reader to measure the signal intensity by the labeled target. Raw data were analyzed with the microarray software (Bead Studio Gene Expression version 3.4.0) for quality control, background analysis and normalization with rank invariant algorithm. Normalized data was further analyzed for comparative molecular and cellular pathway regulation using Ingenuity Pathway Analysis (p=0.05 and delta of 0.19; Quiagen).[44]

Immunohistochemistry

For whole mount immunohistochemistry, eyes were enucleated and fixed in 4% paraformaldehyde at room temperature for 1 h. The retina was isolated and stained for retinal vasculature and lesions with fluoresceinated Isolectin B4 (Alexa Fluor-594 in PBS with $CaCl_2$ 1 mM, I21413, Molecular Probes) overnight at room temperature (RT). Retinas were visualized using a 5× objective with a Zeiss AxioObserver.Z1 microscope, and imaged with a Zeiss AxioCam MRm operated by AxioVision software (version 4.6.3.0). Whole mounts were also fixed and permeabilized in cold methanol (20 min at –20 °C), blocked in 3% bovine serum albumin and 0.1% Triton X-100, stained with Isolectin B_4 to visualize vessels (as above) and/or with primary antibodies against HIF1α (1:100 in TBS, NB00-134, Novus), VEGF (1:100, RB-222, Thermo Scientific), IBA-1 (1:200, CP290A, Biocare Medical UK) and blue opsin cone (1:100, sc-14365, Santa Cruz) overnight at 4 °C, followed

by secondary antibody staining (1 h at RT; AlexaFluor 1:1000, Invitrogen). Flatmounts (and cross-section) were imaged with confocal microscopy (Leica TCS SP2 AOBS) and z-stacks were 3D reconstructed using Volocity software (Perk Elmer).

Western Blot and ELISA

Retinal samples were obtained as described above. Retinal lysate (20 μg) from three different animals or endothelial cells lysate (10 μg) were loaded on an SDS-PAGE gel and electroblotted onto a PVDF membrane. We used retinal nuclear extract (abcam, Ab113474, as per manufacturer's protocol) to enrich Hif1a signals. After blocking, the membranes were incubated with antibodies against β-Actin (Sigma, A1978), Fibrillarin (Cell Signaling, 2639), Hif1a (Novus, NB100-134), and Glut1 (Novus, NB300-666 and Abcam, Ab652), Glut3 (Millipore, AB1344) and Glut4 (Abcam, ab654) overnight (1:1000 each). After washing, membranes were incubated with 1:10,000 horseradish peroxidase-conjugated anti-rabbit or anti-mouse secondary antibodies (Amersham, NA931V and NA934V) for one hour at room temperature. Densitometry was analyzed using ImageJ. Retinal Vegfa concentration was measured by ELISA (as per manual, MMV00, R&D Systems) and normalized by doing a Bradford to measure the total cell protein content of each samples.

Metabolite Profiling

Metabolites of rapidly dissected WT and $Vldlr^{-/-}$ retinas (flash frozen less then a minute from euthanasia; 15–16 biological replicates) were homogenized in 80% methanol (8 μL/mg of tissue) containing the internal standards inosine-$^{15}N_4$, thymine-d_4, and glycocholate-d_4 (Cambridge Isotope Laboratories) using a TissueLyser II (Qiagen) bead mill for 4 minutes at 20 Hz. Samples were centrifuged (9,000 g, 10 min, 4 °C) to pellet debris and supernatants were analyzed using two liquid chromatography tandem mass spectrometry (LC-MS) methods to measure polar metabolites as described previously.[45,46] Briefly, negative ionization mode multiple reaction mode (MRM) data were acquired using an ACQUITY UPLC (Waters) coupled to a 5500 QTRAP triple quadrupole mass spectrometer (AB SCIEX). The supernatants were injected directly onto a 150 × 2.0 mm Luna NH2 column (Phenomenex) that was eluted at a flow rate of 400 μL/min with initial conditions of 10% mobile phase A [20 mM ammonium acetate and 20 mM ammonium hydroxide (Sigma-Aldrich) in water (VWR)] and 90% mobile phase B [10 mM ammonium hydroxide in 75:25 v/v acetonitrile/methanol (VWR)] followed by a 10 min linear gradient to 100% mobile phase A. The ion spray voltage was –4.5 kV and the source temperature was 500°C. Positive ionization mode MRM data were acquired using a 4000 QTRAP triple quadrupole mass spectrometer (AB SCIEX) coupled to an 1100 Series pump (Agilent) and an HTS PAL autosampler (Leap Technologies). Cell extracts (10 μL) were diluted using 40 μL of 74.9:24.9:0.2 (v/v/v) acetonitrile/methanol/formic acid containing stable isotope-labeled internal standards [0.2 ng/μL valine-d8, Isotec; and 0.2 ng/μL phenylalanine-d8 (Cambridge Isotope Laboratories)] and were injected onto a 150 × 2.1 mm Atlantis HILIC column (Waters). The column was eluted isocratically at a flow rate of 250 μL/min with 5% mobile phase A (10 mM ammonium formate and 0.1% formic acid in water) for 1 minute followed by a linear gradient to 40% mobile phase B (acetonitrile with 0.1% formic acid) over 10 minutes. The ion spray voltage was 4.5 kV and the source temperature was 450°C. Raw data were processed using MultiQuant 2.1 (AB SCIEX) for automated peak integration and

metabolite peaks were manually reviewed for quality of integration and compared against known standards to confirm identity.

Photoreceptor (661W) cell culture

Cone photoreceptor cells[47,48] (661W; from Dr. Al-Ubaidi) were cultured as monolayers at 37 °C, 5% CO_2 in a humidified atmosphere in DMEM with FBS 10% supplemented with hydrocortisone (20 μg/500 mL, H-2270, Sigma), Progesterone (20 μg/500 mL, P-8783, Sigma), Putrescine (0.016 g/500 mL, P-7505, Sigma) and β-mercaptoethanol (20 μL/500 mL, M-6250, Sigma). Cells were not contaminated by mycoplasma. Equal number of 661W cells (0.3×10^6) were plated in 6-well dishes and cultured to 80% confluence. Cells were washed twice with PBS, starved for 4 hours (above medium without FBS) then stimulated with GW9508 (14 μM, Cayman) or vehicle. Photoreceptors were then collected 8 hours post-treatment for Hif1a protein expression (see western blot); while their medium was collected at 12 hours for Vegfa quantification by ELISA (as per manual, MMV00, R&D Systems). Vegfa concentration was normalized for the number of cells per well, by doing a Bradford to measure the total cell protein content of each well.

Preparation of AAV2-RK-shVldlr vector and AAV2 virus

Three independent shRNAs against mouse Vldlr were designed using a published algorithm[49]. The template oligonucleotides contain miR-30 microRNA, miR-30 loop and Vldlr shRNA including the sense and the antisense were synthesized (Invitrogen). DNA fragments were amplified, purified, digested and inserted into modified CAG-GFP-miR30 vector (provided by Dr. Zhiqiang Lin and Dr. William T. Pu at Boston Children's Hospital) according to a previous report[50] and CAG promoter was replaced with rhodopsin kinase (RK) promoter[51] that was cloned from pAAV-RK-GFP (provided by Dr. Connie Cepko and Dr. Tiansen Li). The Vldlr knock down efficiency was tested in pup retinas. Recombinant AAV2 vectors were produced as previously described[52]. Briefly, AAV vector, rep/cap packaging plasmid, and adenoviral helper plasmid were mixed with polyethylenimine and transfected into HEK293T cells (CRL-11268, ATCC). Seventy-two hours after transfection, cells were harvested and the cell pellet was resuspended in virus buffer, followed by 3 cycles of freeze-thaw, and homogenized. Cell debris was pelleted at 5,000 g for 20 minutes, and the supernatant was run on an iodixanol gradient. Recovered AAV vectors were washed 3 times with PBS using Amicon 100K columns (EMD Millipore). Real-time PCR was used to determine genome titers of the recombinant AAV. This protocol also was used to prepare a control AAV2-shControl. Viruses were diluted to various concentrations to test infection, and a concentration of approximately 2×10^{12} gc/mL was used for the experiments. The sequences of the mouse Vldlr siRNAs are as follows: shVldlr #1 (5'-3'), GGA AAG TTC AAG TGC AGA AGC G; shVldlr #2 (5'-3'), GGA ATG CCA TAT CAA CGA ATG C; shVldlr #3 (5'-3'), GGG ATC TGC AGT CAA ATT TGT A; Scramble shRNA control (5'-3'), GAT TTA AGA CAA GCG TAT AAC A.

Human samples and vitrectomy

The study conforms to the tenets of the Declaration of Helsinki, and approval of the human clinical protocol and informed consent were obtained from the Maisonneuve-Rosemont Hospital (HMR) ethics committee (Ref. CER: 10059). All patients previously diagnosed

with AMD were followed and surgery was performed by a single vitreoretinal surgeon (F.A.R.). Vitreous samples were frozen on dry ice immediately after biopsy and stored (−80 °C). VEGFA ELISAs were performed according to manufacturer's instructions (DVE00, R&D Systems).

Statistical analysis

We used Student's *t*-test, and ANOVA with *Dunnet, Bonferroni or Tukey* post-hoc analysis (see Supplementary Table 2), to compare different groups; p<0.05 was considered statistically different. *D'Agostino-Pearson* or *Kolmogorov-Smirnov* (KS) normality test were used to confirm normal distribution. Data with non-*Gaussian* distribution was analysed using a *Mann Whitney* test (non-parametric, two groups). Animals were not randomized but quantifications were blinded when possible. All experiments were repeated at least 3 times. Values more than 2 standard deviations from the mean were considered outliers and were excluded. Sample size was estimated to detect a difference of 20% with a power of 80% (1-β) and α of 0.05 in accordance with the 'Guidelines for the Use of Animals in Neuroscience' (2003). Results are presented as mean ± SEM. * $P < 0.05$, ** $P < 0.01$, *** $P < 0.001$.

Supplementary Material

Refer to Web version on PubMed Central for supplementary material.

Acknowledgments

References

REFERENCES

1. Cahill GF. Starvation in man. N Engl J Med. 1970; 282:668–675. [PubMed: 4915800]
2. Wong-Riley MTT. Energy metabolism of the visual system. Eye Brain. 2010; 2:99–116. [PubMed: 23226947]
3. Cohen LH, Noell WK. Glucose catabolism of rabbit retina before and after development of visual function. J Neurochem. 1960; 5:253–276. [PubMed: 13810977]
4. Niu Y-G, Evans RD. Very-low-density lipoprotein: complex particles in cardiac energy metabolism. J Lipids. 2011; 2011:189876. [PubMed: 21773049]
5. Goudriaan JR, et al. The VLDL receptor plays a major role in chylomicron metabolism by enhancing LPL-mediated triglyceride hydrolysis. J Lipid Res. 2004; 45:1475–1481. [PubMed: 15145981]
6. Dorrell MI, et al. Antioxidant or neurotrophic factor treatment preserves function in a mouse model of neovascularization-associated oxidative stress. J Clin Invest. 2009; 119:611–623. [PubMed: 19188685]

7. Bottoni F, et al. Treatment of retinal angiomatous proliferation in age-related macular degeneration: a series of 104 cases of retinal angiomatous proliferation. Arch Ophthalmol. 2005; 123:1644–1650. [PubMed: 16344434]

8. Yannuzzi LA, et al. Idiopathic macular telangiectasia. Retina. 2012; 32(Suppl 1):450–460. [PubMed: 22451954]

9. Lim LS, Mitchell P, Seddon JM, Holz FG, Wong TY. Age-related macular degeneration. Lancet. 2012; 379:1728–1738. [PubMed: 22559899]

10. Okawa H, Sampath AP, Laughlin SB, Fain GL. ATP consumption by mammalian rod photoreceptors in darkness and in light. Curr Biol. 2008; 18:1917–1921. [PubMed: 19084410]

11. Mantych GJ, Hageman GS, Devaskar SU. Characterization of glucose transporter isoforms in the adult and developing human eye. Endocrinology. 1993; 133:600–607. [PubMed: 8344201]

12. Gospe SM, Baker SA, Arshavsky VY. Facilitative glucose transporter Glut1 is actively excluded from rod outer segments. J Cell Sci. 2010; 123:3639–3644. [PubMed: 20923839]

13. Klepper J. Glucose transporter deficiency syndrome (GLUT1DS) and the ketogenic diet. Epilepsia. 2008; 49(Suppl 8):46–49. [PubMed: 19049586]

14. Lopaschuk GD, Ussher JR, Folmes CDL, Jaswal JS, Stanley WC. Myocardial fatty acid metabolism in health and disease. Physiol Rev. 2010; 90:207–258. [PubMed: 20086077]

15. Obunike JC, et al. Transcytosis of lipoprotein lipase across cultured endothelial cells requires both heparan sulfate proteoglycans and the very low density lipoprotein receptor. J Biol Chem. 2001; 276:8934–8941. [PubMed: 11121409]

16. Tyni T, Paetau A, Strauss AW, Middleton B, Kivelä T. Mitochondrial fatty acid beta-oxidation in the human eye and brain: implications for the retinopathy of long-chain 3-hydroxyacyl-CoA dehydrogenase deficiency. Pediatr Res. 2004; 56:744–750. [PubMed: 15347768]

17. Sarac O, Gulsuner S, Yildiz-Tasci Y, Ozcelik T, Kansu T. Neuro-ophthalmologic findings in humans with quadrupedal locomotion. Ophthalmic Genet. 2012; 33:249–252. [PubMed: 22686558]

18. Trick GL, Berkowitz BA. Retinal oxygenation response and retinopathy. Prog Retin Eye Res. 2005; 24:259–274. [PubMed: 15610976]

19. Furukawa T, Morrow EM, Cepko CL. Crx, a novel otx-like homeobox gene, shows photoreceptor-specific expression and regulates photoreceptor differentiation. Cell. 1997; 91:531–541. [PubMed: 9390562]

20. Winkler BS. Glycolytic and oxidative metabolism in relation to retinal function. J Gen Physiol. 1981; 77:667–692. [PubMed: 6267165]

21. Hu W, et al. Expression of VLDLR in the retina and evolution of subretinal neovascularization in the knockout mouse model's retinal angiomatous proliferation. Invest Ophthalmol Vis Sci. 2008; 49:407–415. [PubMed: 18172119]

22. Lefebvre P, Chinetti G, Fruchart J-C, Staels B. Sorting out the roles of PPAR alpha in energy metabolism and vascular homeostasis. J Clin Invest. 2006; 116:571–580. [PubMed: 16511589]

23. Nakamura MT, Yudell BE, Loor JJ. Regulation of energy metabolism by long-chain fatty acids. Prog Lipid Res. 2014; 53:124–144. [PubMed: 24362249]

24. Itoh Y, et al. Free fatty acids regulate insulin secretion from pancreatic beta cells through GPR40. Nature. 2003; 422:173–176. [PubMed: 12629551]

25. Kebede M, et al. The fatty acid receptor GPR40 plays a role in insulin secretion in vivo after high-fat feeding. Diabetes. 2008; 57:2432–2437. [PubMed: 18559658]

26. Alquier T, et al. Deletion of GPR40 impairs glucose-induced insulin secretion in vivo in mice without affecting intracellular fuel metabolism in islets. Diabetes. 2009; 58:2607–2615. [PubMed: 19720802]

27. Steneberg P, Rubins N, Bartoov-Shifman R, Walker MD, Edlund H. The FFA receptor GPR40 links hyperinsulinemia, hepatic steatosis, and impaired glucose homeostasis in mouse. Cell Metab. 2005; 1:245–258. [PubMed: 16054069]

28. Honoré J-C, et al. Fatty acid receptor Gpr40 mediates neuromicrovascular degeneration induced by transarachidonic acids in rodents. Arterioscler Thromb Vasc Biol. 2013; 33:954–961. [PubMed: 23520164]

29. Briscoe CP, et al. The orphan G protein-coupled receptor GPR40 is activated by medium and long chain fatty acids. J Biol Chem. 2003; 278:11303–11311. [PubMed: 12496284]

30. Naik H, et al. Safety, Tolerability, Pharmacokinetics, and Pharmacodynamic Properties of the GPR40 Agonist TAK-875: Results From a Double-Blind, Placebo-Controlled Single Oral Dose Rising Study in Healthy Volunteers. J Clin Pharmacol. 2012; 52:1007–1016. [PubMed: 21610201]

31. Kaelin WG. Cancer and altered metabolism: potential importance of hypoxia-inducible factor and 2-oxoglutarate-dependent dioxygenases. Cold Spring Harb Symp Quant Biol. 2011; 76:335–345. [PubMed: 22089927]

32. Hua J, et al. Resveratrol inhibits pathologic retinal neovascularization in Vldlr(−/−) mice. Investigative ophthalmology & visual science. 2011; 52:2809–2816. [PubMed: 21282584]

33. Ohno-Matsui K, et al. Inducible expression of vascular endothelial growth factor in adult mice causes severe proliferative retinopathy and retinal detachment. The American journal of pathology. 2002; 160:711–719. [PubMed: 11839592]

34. Zhou X, Wong LL, Karakoti AS, Seal S, McGinnis JF. Nanoceria inhibit the development and promote the regression of pathologic retinal neovascularization in the Vldlr knockout mouse. PloS one. 2011; 6:e16733. [PubMed: 21364932]

35. Chen Y, et al. Photoreceptor degeneration and retinal inflammation induced by very low-density lipoprotein receptor deficiency. Microvasc Res. 2009; 78:119–127. [PubMed: 19281829]

36. Fletcher AL, Pennesi ME, Harding CO, Weleber RG, Gillingham MB. Observations regarding retinopathy in mitochondrial trifunctional protein deficiencies. Molecular Genetics and Metabolism. 2012; 106:18–24. [PubMed: 22459206]

37. Ferrannini E, Barrett EJ, Bevilacqua S, DeFronzo RA. Effect of fatty acids on glucose production and utilization in man. J Clin Invest. 1983; 72:1737–1747. [PubMed: 6138367]

38. Wauson EM, Lorente-Rodríguez A, Cobb MH. Minireview: Nutrient sensing by G protein-coupled receptors. Mol Endocrinol. 2013; 27:1188–1197. [PubMed: 23820899]

39. Warburg O. On the origin of cancer cells. Science. 1956; 123:309–314. [PubMed: 13298683]

40. Zhao S, et al. Glioma-derived mutations in IDH1 dominantly inhibit IDH1 catalytic activity and induce HIF-1alpha. Science. 2009; 324:261–265. [PubMed: 19359588]

METHODS-ONLY REFERENCES

41. Stahl A, et al. Postnatal weight gain modifies severity and functional outcome of oxygen-induced proliferative retinopathy. Am J Pathol. 2010; 177:2715–2723. [PubMed: 21056995]

42. Stahl A, et al. Computer-aided quantification of retinal neovascularization. Angiogenesis. 2009; 12:297–301. [PubMed: 19757106]

43. Spahis S, et al. Plasma fatty acid composition in French-Canadian children with non-alcoholic fatty liver disease: Effect of n-3 PUFA supplementation. Prostaglandins Leukot Essent Fatty Acids. 2015; 99:25–34. [PubMed: 26066299]

44. Calvano SE, et al. A network-based analysis of systemic inflammation in humans. Nature. 2005; 437:1032–1037. [PubMed: 16136080]

45. Jain M, et al. Metabolite profiling identifies a key role for glycine in rapid cancer cell proliferation. Science. 2012; 336:1040–1044. [PubMed: 22628656]

46. Townsend MK, et al. Reproducibility of metabolomic profiles among men and women in 2 large cohort studies. Clin Chem. 2013; 59:1657–1667. [PubMed: 23897902]

47. al-Ubaidi MR, et al. Bilateral retinal and brain tumors in transgenic mice expressing simian virus 40 large T antigen under control of the human interphotoreceptor retinoid-binding protein promoter. J Cell Biol. 1992; 119:1681–1687. [PubMed: 1334963]

48. Tan E, et al. Expression of cone-photoreceptor-specific antigens in a cell line derived from retinal tumors in transgenic mice. Invest Ophthalmol Vis Sci. 2004; 45:764–768. [PubMed: 14985288]

49. Park YK, et al. AsiDesigner: exon-based siRNA design server considering alternative splicing. Nucleic acids research. 2008; 36:W97–W103. [PubMed: 18480122]

50. Grieger JC, Choi VW, Samulski RJ. Production and characterization of adeno-associated viral vectors. Nature protocols. 2006; 1:1412–1428. [PubMed: 17406430]

51. Khani SC, et al. AAV-mediated expression targeting of rod and cone photoreceptors with a human rhodopsin kinase promoter. Investigative ophthalmology & visual science. 2007; 48:3954–3961. [PubMed: 17724172]

52. Vandenberghe LH, et al. Efficient serotype-dependent release of functional vector into the culture medium during adeno-associated virus manufacturing. Human gene therapy. 2010; 21:1251–1257. [PubMed: 20649475]
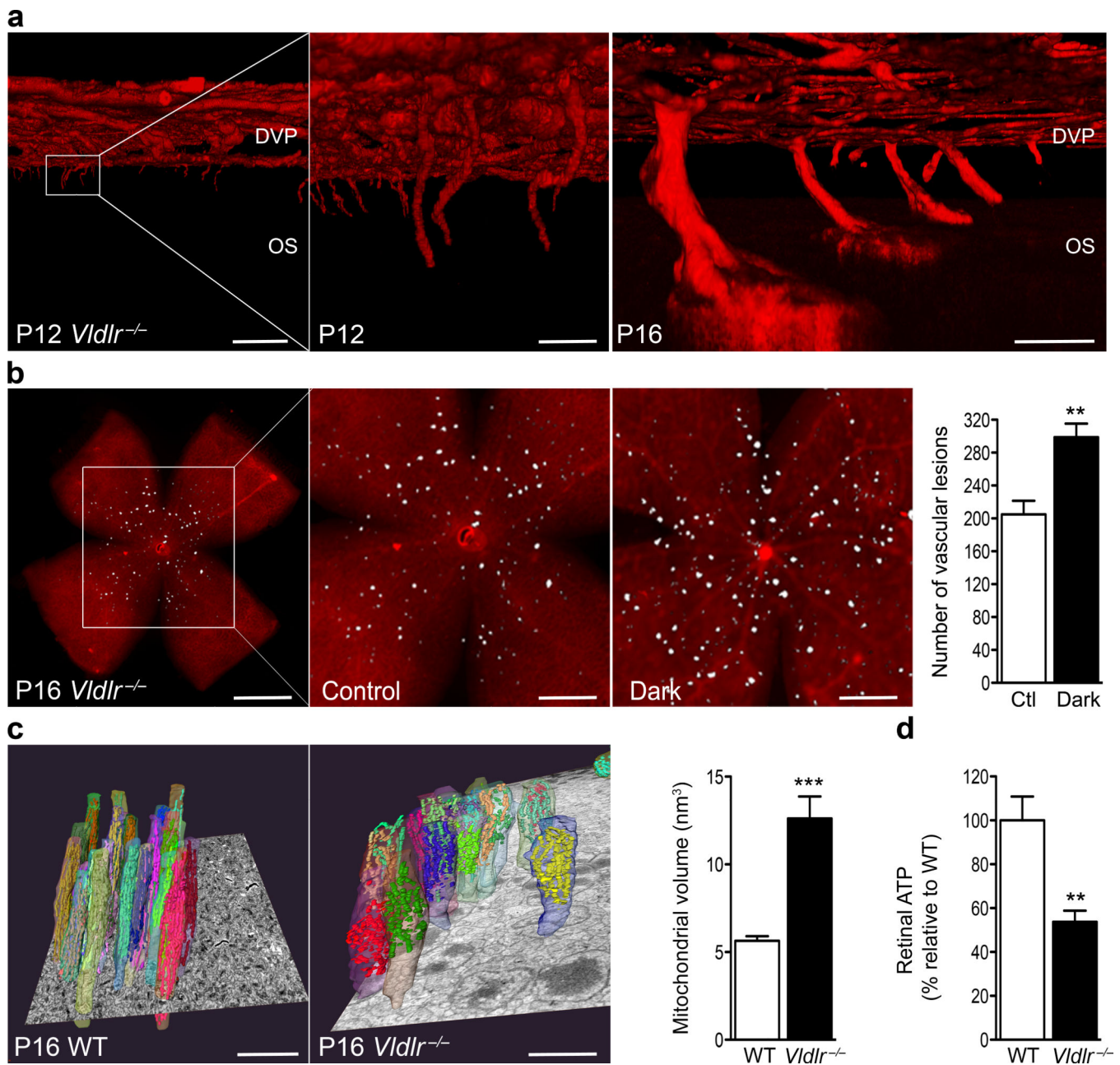
Figure 1. Retinal energy deficits are associated with vascular lesions in *Vldlr*$^{-/-}$

(**a**) Pathologic vessels in *Vldlr*$^{-/-}$ retinas originated from the deep vascular plexus (DVP) and breached the outer plexiform layer (P12), extending towards photoreceptor outer segments (os) at P16. Scale: 200 μm. n = 5 retinas. (**b**) *Vldlr*$^{-/-}$ pups raised in darkness (n = 10 retinas) compared to normal 12 hours light/dark cycle (Ctl: control, n = 28) to increase retinal energy demands. Scale: 1 mm (left), 0.5 mm (others). White spots label vascular lesions. *P* = 0.0031. (**c**) Mitochondrial volume quantified by 3D reconstruction of retinal scanning electron microscopy (SEM) images. Mitochondria within photoreceptors are pseudo-colored. n = 23 photoreceptors. Scale: 5μm. *P* < 0.0001. (**d**) Retinal ATP level was significantly lower in *Vldlr*$^{-/-}$ retina (n = 6) compared to littermate control wild type retinas

(WT; n = 4). $P = 0.0026$. Results are presented as mean ± SEM. Two-tailed Student t-test; ** $P < 0.01$, *** $P < 0.001$.
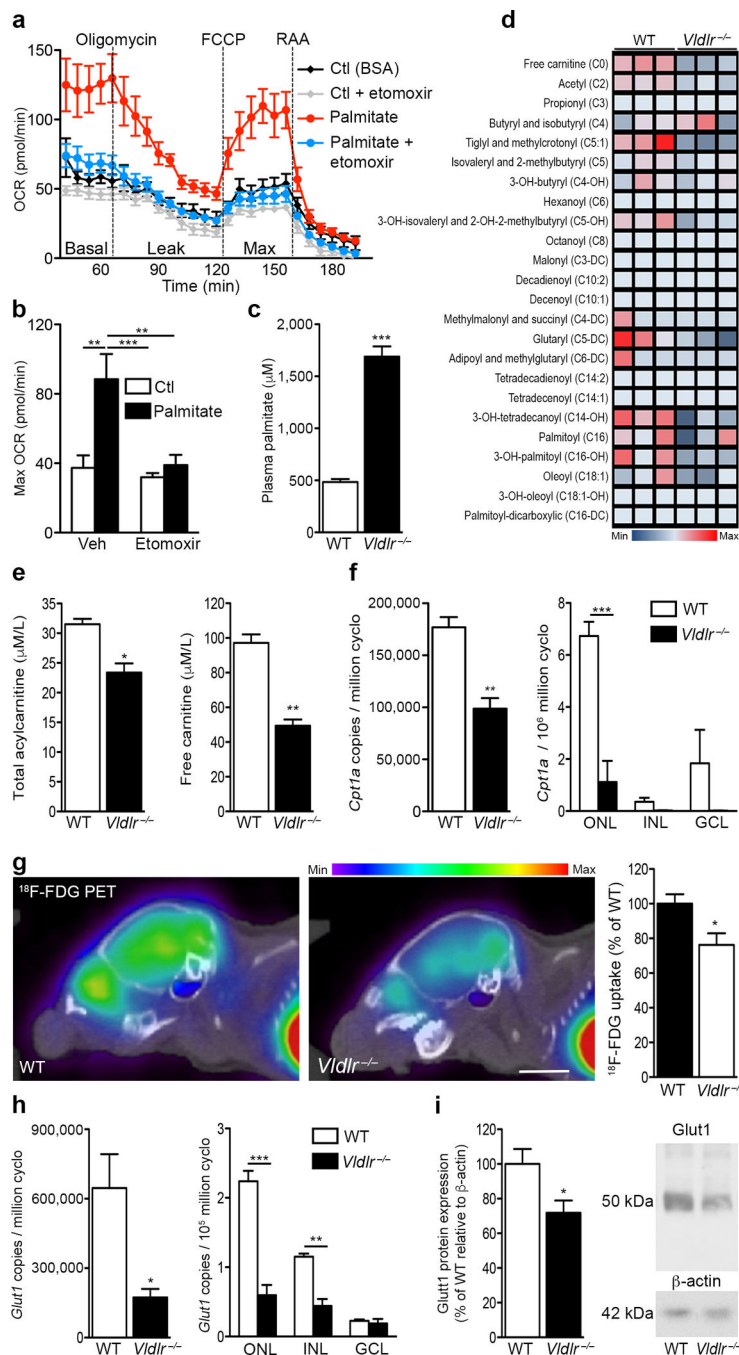
Figure 2. Dual lipid and glucose fuel deficiency in *Vldlr*−/− retinas
(**a**) Oxygen consumption rate (OCR) and (**b**) maximal OCR of wild type (WT) retinas provided with long-chain fatty acid (FA) palmitate or control (Ctl: bovine serum albumin or BSA) in the presence or absence of FA oxidation inhibitor, etomoxir (40 μM). n = 6–8 retinas. (**c**) Circulating plasma palmitate levels in WT and *Vldlr*−/− mice. n = 7 WT, 13 *Vldlr*−/− mice plasma samples. *P*<0.0001. (**d**) Metabolite array of FA β-oxidation, (**e**) total acylcarnitine (*P* = 0.0108) and free carnitine levels (*P* = 0.0014) measured by LC/MS/MS. n = 3 animal retinas. (**f**) *Cpt1a* mRNA expression of intact retinas (left; *P* = 0.0052) and laser

capture microdissected (LCM) retinal layers by qRT-PCR. ONL: outer nuclear (photoreceptors); INL: inner nuclear and GCL: ganglion cell layers. n = 3 animal retinas. (**g**) ^{18}F-FDG microPET and CT scan revealed decreased glucose uptake in *Vldlr*$^{-/-}$ retinas, confirmed by retinal gamma radioactivity counts. Scale: 4 mm. n = 22 WT, 12 *Vldlr*$^{-/-}$ retinas, $P = 0.0116$. (**h**) *Glut1* mRNA expression in intact retinas (left, n = 9 WT, 12 *Vldlr*$^{-/-}$ retinas; $P = 0.0119$) and retinal layers (right) by LCM and qRT-PCR (n = 3 retinas). (**i**) Glut1 protein expression of intact WT and *Vldlr*$^{-/-}$ retina. n = 6 retinas, $P = 0.030$. Results are presented as mean ± SEM. Two-tailed Student *t*-test (**c–f**, **g–i**) and one-way ANOVA with *Tukey* post-hoc analysis (**b,f,h**); * $P < 0.05$, ** $P < 0.01$, *** $P < 0.001$.
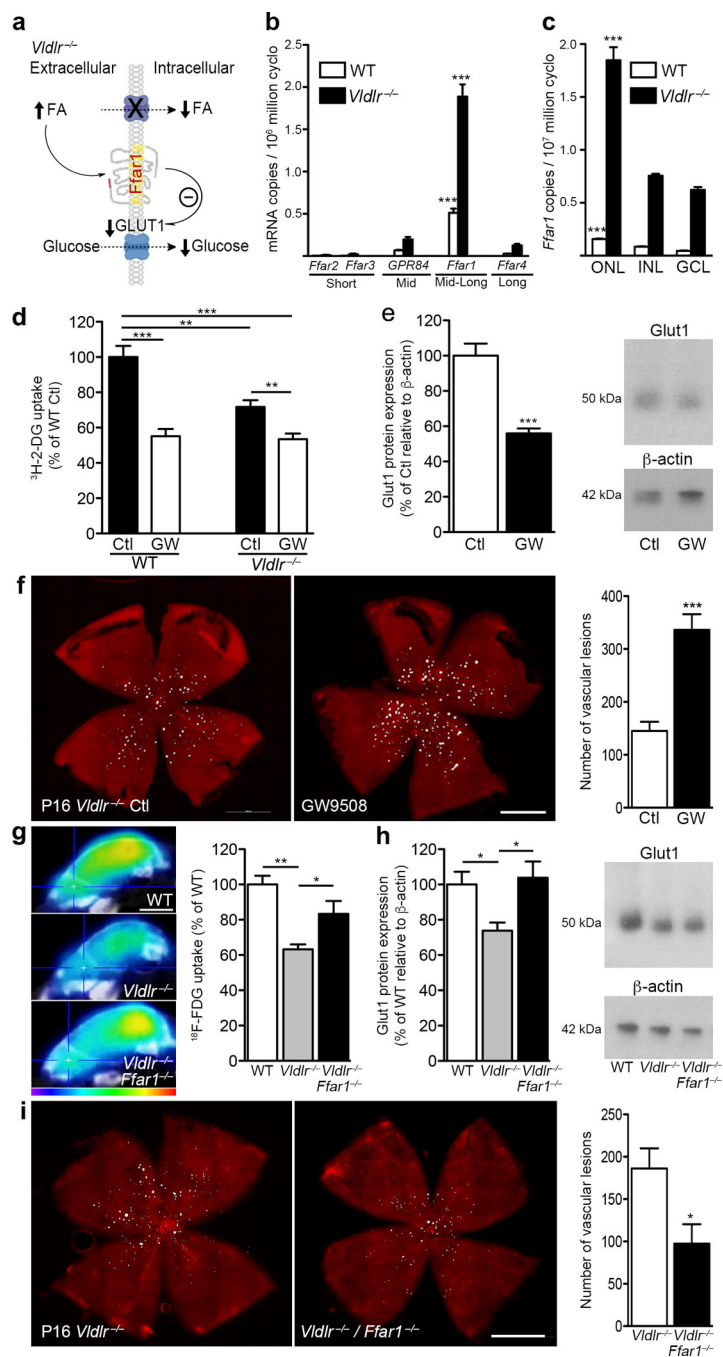
Figure 3. Ffar1 modulates retinal glucose uptake and RAP

(**a**) Decreased lipid uptake in *Vldlr*^{−/−} retina increased extracellular mid/long chain FA, the agonist of lipid sensor Ffar1, which was associated with reduced Glut1 expression. (**b**) Expression of FA sensing GPCR in WT and *Vldlr*^{−/−} intact retinas and (**c**) Ffar1 distribution in retinal layers by LCM (qRT-PCR). ONL: outer nuclear layer, INL: inner nuclear layer, GCL: ganglion cell layer. n = 3 animal retinas. (**d**) Glucose uptake (^{3}H-2-DG tracer; n = 5–8 ctl, 9–16 GW-treated retinas), (**e**) Glut1 protein expression (n = 12 retinas, $P < 0.0001$) and (**f**) number of RAP-like pathologic vascular lesions at P16 in WT and *Vldlr*^{−/−} mice treated

with Ffar1 agonist GW9508 (GW; n = 11) or vehicle (ctl; n = 7, P = 0.0002). (**g**) Glucose uptake (^{18}F-FDG; n = 4 retinas, scale: 4 mm), (**h**) Glut1 protein expression (n = 10 WT, others 9 retinas), and (**i**) number of RAP-like pathologic vascular lesions of WT (no lesions) and $Vldlr^{-/-}$ mice compared to littermate $Vldlr^{-/-}/Ffar1^{+/+}$ mice (P16; n = 10 retinas, P = 0.0153). Results are presented as mean ± SEM. Two-tailed Student t-test (**e,f,i**) and one-way ANOVA with *Dunnett's* (**b,c,g,h**) or *Tukey's* (**d**) post-hoc comparison; * P < 0.05, ** P < 0.01, *** P < 0.001.
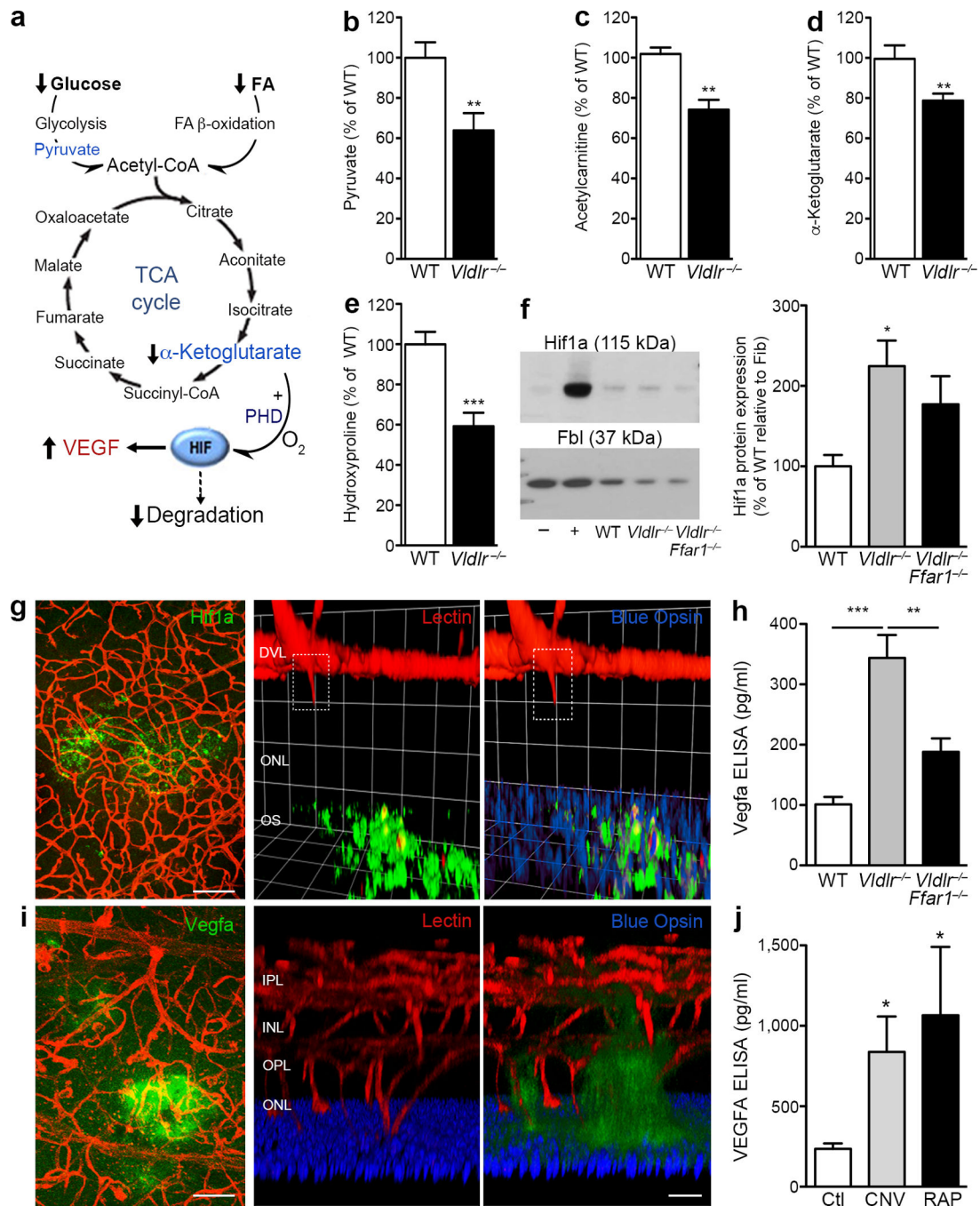
Figure 4. Fuel deficient *Vldlr*⁻/⁻ retina generates less α-Ketoglutarate and more Vegf
(**a**) Dual shortage of glucose (**b**, pyruvate; n = 15 WT, 12 *Vldlr*⁻/⁻ retinas *P* = 0.0032) and
FA uptake reduces acetyl-coA (**c**, estimated by measuring acetylcarnitine; n = 3, *P* = 0.0094)
and (**d**) TCA (Krebs) cycle intermediate α-KG in *Vldlr*⁻/⁻ retina (LC/MS/MS; n = 11 WT,
15 *Vldlr*⁻/⁻ retinas, *P* = 0.0069). Together with oxygen (O₂), α-KG is an essential co-
activator of propyl-hydroxylase dehydrogenase (PHD) that tags HIF-1α for degradation by
proline hydroxylation (hydroxyproline). (**e**) Levels of hydroxyproline residues in WT and
Vldlr⁻/⁻ retinas measured by LC/MS/MS (n = 15 WT, 12 *Vldlr*⁻/⁻ animal retinas, *P* =

0.0004) and (**f**) Hif1a stabilization of WT, *Vldlr*$^{-/-}$ and *Vldlr*$^{-/-}$/*Ffar1*$^{-/-}$ retinal nuclear extractions. We used Fibrillarin (Fbl) as nuclear loading control. n = 3 all groups. (**g**) Hif1a retinal expression in *Vldlr*$^{-/-}$ photoreceptor layer (P12 retinal flat mounts, Scale: 100 μm; left: extended focus; middle and right panels: 3D confocal IHC, n = 3) where (**h**) Vegfa was then also secreted (P16, ELISA, n = 6 retinas) and (**i**) localized (P16 retinal flat mounts, Scale: 100 μm; left: extended focus; middle and right panels: 3D confocal IHC, n = 3 retinas). (**j**) Human subjects with AMD, either retinal angiomatous proliferation (RAP, n = 3) or choroidal neovascularization (CNV, n = 7) had higher VEGFA vitreous levels by ELISA compared to control subjects without pathologic neovessels (macular hole; n = 8). Results are presented as mean ± SEM. Two-tailed Student *t-test* (**c,d**), *Mann Whitney* test (**b,e**), and one-way ANOVAs with post-hoc *Dunett's* (**f,j**) *or Tukey's* multiple comparison (**h**); * *P* < 0.05, ** *P* < 0.01, *** *P* < 0.001.